§22. Statistical Analysis of Non-Diffusive Transport in Edge Plasmas of the LHD Device

Ohno, N., Tsuji, Y. (Nagoya Univ.),
Budaev, V. (Kuruchatov Institute),
Dendy, R. (Culham Science Centre),
Masuzaki, S., Komori, A., Morisaki, T., Ohyabu, N.

We investigated the ion saturation current $I_{\rm sat}$ signals measured using a Langmuir probe array embedded in a divertor plate as shown in Fig. 1(a). The sampling frequency was 500 kHz. Figure 1(b) shows a profile of the connection length of the magnetic field line, $L_{\rm c}$. The positions of the Langmuir probes are also shown in Fig. 1(b). The maximum length of $L_{\rm c}$ exceeds 1 km, and the strike point of LHD is defined at around the peak position of the $L_{\rm c}$ profile. Probe ♯10 is closest to the strike point. The private side, corresponding to the LFS on the divertor plate, coincides with the direction in which the probe number is small.

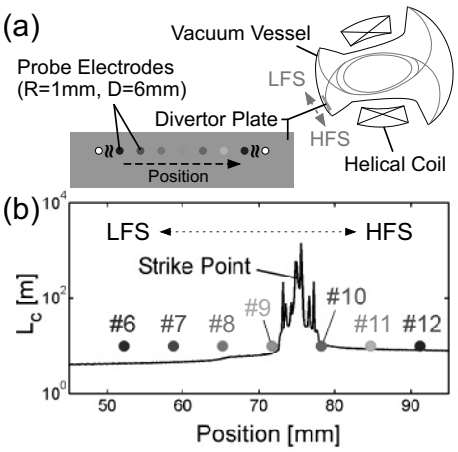

Fig. 1: (a) Cross-section in LHD and a scheme of the Langmuir probe array on the divertor plate, and (b) a distribution of the magnetic field length $L_{\rm c}$ on the divertor plate.

Figure 2 shows the power spectra, $S(f)$, at probes ♯9 and 10 in the attached- and detached-states. In the attached-state, $S(f)$ obeys three types of power-law distributions ($S(f) \sim f^{-\alpha}$) at (i) a frequency lower than 3.3 kHz, (ii) higher than 3.3 kHz and lower than 20 kHz, and (iii) higher than 20 kHz. In type (i), the $S(f)$ profiles at both probes are almost flat. Relatively large exponents α are observed for type (iii) as compared to those for type (ii). In order to obtain a more sharp profile of $S(f)$ at probe ♯10, a long time signal (600 ms $< t <$ 1000 ms) is also calculated, as shown in Fig. 2(b), at the expense of a reduction in the magnitude accuracy due to the influence of the limitation of the $I_{\rm sat}$ signal. The spectrum

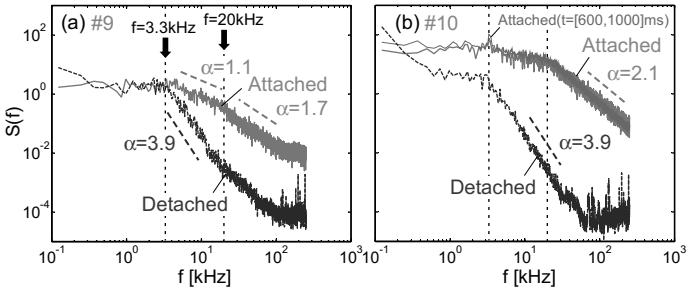

Fig. 2: Power spectra of $I_{\rm sat}$ signals at probes (a) *sharp*9 and (b) ♯10 in the attached- and detached-states.

exhibits a relatively small peak at the frequency of 3.3 kHz.

In the detached-state, $S(f)$ has a convex shape in the low-frequency region around 100 Hz at probe ♯10, as shown in Fig. 2(b), possibly due to the serpens mode. Above 3.3 kHz, the shapes of the $S(f)$ curves obey the power-law distribution with a large exponent ($\alpha = 3.9$), and the higher-frequency components reach background levels. At the frequency of 3.3 kHz, the shoulders of the $S(f)$ curves are clearly observed in this state. The frequency at a shoulder corresponds to approximately the inverse of the time scale of the burst duration. The shoulder appears when the duration of the dominant spikes is uniform and spikes occur non-periodically. The power spectra at the other probes ♯6–8 and ♯11 in this state exhibit properties similar to those at probe ♯9 and ♯10, respectively.

In order to reveal the profile of a typical burst at probe ♯9, the conditional averaging method is employed. Large spikes with peaks that are more than two times as large as the standard deviation are extracted and averaged in the same time domain. Figure 3 shows the conditional-averaged fluctuation components of $I_{\rm sat}$ in the attached- and detached-states. In the attached-state, the averaged positive spike exhibits a rapid increase and a slow decay. In contrast, the averaged shape in the detached-state exhibits a gradual feature, and its duration time scale is longer than that in the attached-state.

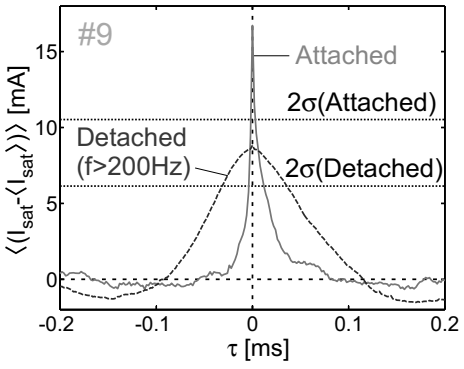

Fig. 3: Conditional averaging results of $I_{\rm sat}$ at probe ♯9 in the attached- and detached-states .